Transition to seizure in focal epilepsy: From <scp>SEEG</scp> phenomenology to underlying mechanisms

Mehmet Alihan Kayabas, Elif Köksal Ersöz, Maxime Yochum, Fabrice Bartolomei, Pascal Benquet, Fabrice Wendling

Received: 31 May 2024 | Revised: 15 October 2024 | Accepted: 15 October 2024

DOI: 10.1111/epi.18173

Epilepsia®

RESEARCH ARTICLE

Transition to seizure in focal epilepsy: From SEEG phenomenology to underlying mechanisms

Mehmet Alihan Kayabas[1] | **Elif Köksal Ersöz**[1] | **Maxime Yochum**[1] | **Fabrice Bartolomei**[2,3] | **Pascal Benquet**[1] | **Fabrice Wendling**[1]

[1]INSERM, LTSI U1099, Université de Rennes, Rennes, France

[2]Epileptology and Cerebral Rhythmology, Timone Hospital, APHM, Marseille, France

[3]Univ Aix Marseille, INSERM, INS, Inst Neurosci Syst, Marseille, France

Correspondence
Fabrice Wendling, LTSI, Inserm U1099, Université de Rennes, Campus de Beaulieu, Bât. 22, Rennes 35042, France.
Email: fabrice.wendling@inserm.fr

Funding information
H2020 European Research Council, Grant/Award Number: 855109

Abstract

Objective: For the pre-surgical evaluation of patients with drug-resistant focal epilepsy, stereo-electroencephalographic (SEEG) signals are routinely recorded to identify the epileptogenic zone network (EZN). This network consists of remote brain regions involved in seizure initiation. However, the pathophysiological mechanisms underlying typical SEEG patterns that occur during the transition from interictal to ictal activity in distant brain nodes of the EZN remain poorly understood. The primary aim is to identify and explain these mechanisms using a novel physiologically-plausible model of the EZN.

Methods: We analyzed SEEG signals recorded from the EZN in 10 patients during the transition from interictal to ictal activity. This transition consisted of a sequence of periods during which SEEG signals from distant neocortical regions showed stereotypical patterns of activity: sustained preictal spiking activity preceding a fast activity occurring at seizure onset, followed by the ictal activity. Spectral content and non-linear correlation of SEEG signals were analyzed. In addition, we developed a novel neuro-inspired computational model consisting of bidirectionally coupled neuronal populations.

Results: The proposed model captured the essential characteristics of the patient signals, including the quasi-synchronous onset of rapid discharges in distant interconnected epileptogenic zones. Statistical analysis confirmed the dynamic correlation/de-decorrelation pattern observed in the patient signals and accurately reproduced in the simulated signals.

Significance: This study provides insight into the abnormal dynamic changes in glutamatergic and γ-aminobutyric acid (GABA)ergic synaptic transmission that occur during the transition to seizures. The results strongly support the hypothesis that bidirectional connections between distant neuronal populations of the EZN (from pyramidal cells to vaso-intestinal peptide-positive interneurons) play a key role in this transition, while parvalbumin-positive interneurons intervene in the emergence of rapid discharges at seizure onset.

KEYWORDS
epilepsy, fast-onset activity, ictal activity, interictal-ictal transition, model-based interpretation, neural mass model, pre-ictal spikes, synchronization pattern

1 | INTRODUCTION

In patients with focal drug-resistant epilepsy, the epileptogenic zone network (EZN) also known as the "seizure-onset zone," is often organized as a network of interconnected distant brain regions involved in seizure initiation and propagation. In these patients, intracerebral recordings with stereo-electroencephalographic (SEEG) electrodes are used to precisely delineate the EZN.[1] Several seizure-onset patterns have been identified from SEEG recordings,[2] with several modes of transition from the interictal to the ictal period.

One of the most typical patterns shows a sequence of activity during the transition to seizure: (i) the interictal period with sporadic spikes, (ii) the pre-ictal period with large-amplitude rhythmic spikes, (iii) the low-voltage fast activity hallmarked by gamma-band oscillations (24–80 Hz), (iv) the ictal activity with sustained spikes (5–15 Hz) during which the seizure spreads to other brain regions, and, finally, (v) the seizure termination, which is often abrupt. Among these activities, fast-onset activity (FOA, also referred to as rapid discharge or fingerprint[3]) has long been considered a marker of seizure onset in human neocortical and mesial temporal epilepsies,[4] and has been the topic of increasing interest over the last three decades.[3,5–8] As a result, FOA is now considered a reliable marker of the seizure-onset zone.

Although the above sequence of activity is commonly observed, the pathophysiological mechanisms underlying the successive transitions are poorly understood. In addition, the quasi-simultaneous occurrence of low-voltage fast activity in distant brain regions remains puzzling, in a context where the analysis of SEEG signals has provided evidence of desynchronization between involved brain structures at seizure onset.[6]

In this study, we report the results of analysis and computational modeling of SEEG signals recorded during the interictal-to-ictal transition in 10 patients with drug-resistant epilepsy.

From a modeling perspective, we present a novel neurophysiologically plausible model of two coupled neocortex regions that provides mechanistic insights into the neuronal circuits involved in the transition to seizure. In particular, with regard to the mechanisms implicated in the generation of FOA, the model highlights the increased firing of fast spiking γ-aminobutyric acid (GABA)ergic interneurons at seizure onset, in line with in vivo[7] and in vitro[9] electrophysiological, and optogenetic studies.[10,11]

Key points

- The mechanisms underlying the transition to epileptic activity in remote regions of the epileptic zone network (EZN) remain poorly understood.
- This study investigates these mechanisms using a novel neuro-inspired computational model combined with signal processing.
- It shed light on the dynamic changes in glutamatergic and γ-aminobutyric acid (GABA)ergic synaptic transmission during the transition to seizures.
- It brings evidence on the role of connections between remote neuronal populations and the involvement of specific types of interneurons.
- The identified mechanisms could lead to improved strategies for presurgical evaluation in patients with drug-resistant focal epilepsy.

Of interest, the model predicts that the depolarizing GABA mechanism[12] implemented at the level of the fast-spiking GABAergic interneurons not only plays a role in the FOA frequency but also in the decrease of this frequency with time (so-called chirping phenomenon).

From a signal analysis perspective, this study introduces a novel statistical approach to assess differences in the correlation between SEEG signals during the successive phases of the interictal–ictal transition. It adds further evidence on the existence of a "synchronization, de-synchronization, re-synchronization" pattern, hypothesized to be a hallmark of the seizure-onset zone.[6,13,14] This pattern is accurately reproduced in simulated SEEG signals by fine-tuning the model parameter values.

To the best of our knowledge, this study is the first to accurately model the sequence of pathophysiological mechanisms at the origin of the electrophysiological patterns observed during the interictal–ictal transition in focal epilepsies.

2 | MATERIALS AND METHODS

2.1 | SEEG data description

A data subset of SEEG signals recorded in $n=10$ patients (Table SI1.1) was extracted from a larger data set ($n=70$

patients) collected for the project named "EEG-Process" ("Retrospective analysis of EEG signals collected in routine care during the evaluation of epileptic patients", ref. RCAPHM23_0012). This project was approved by legal entities including the institutional review board (IRB00003888, IORG0003254, and FWA00005831) of the French National Institute of Health and Medical Research (Inserm). The recordings were performed at the epilepsy department of La Timone University Hospital, Marseille, France. Selected signals were recorded from multi-contact intracerebral electrodes implanted in the brain according to Talairach's stereotactic method,[15] as illustrated in Figure 1A. In this study, bipolar signals were used, which were obtained by subtracting monopolar signals recorded on two adjacent contacts of the electrodes (identified by capital letters, e.g., SA for Supplementary Area and numbered from 1 to 15, with lower numbers indicating mesial structures and higher numbers indicating lateral structures). The electrode geometry is shown in Figure 1B. As exemplified in Figure 1C, selected SEEG signals showed characteristic transitions from interictal to ictal periods. In the 10 selected patients, we confirmed that the interictal-to-ictal transition patterns were reproducible in each patient, as reported in a previous study.[16] One seizure per patient was selected on the basis of visual inspection. Selection criteria were: (i) SEEG signals are recorded from distant neocortical regions (Table SI1); (ii) selected bipolar signals showed typical patterns of interictal to ictal transition, including distinct pre-ictal (PreICT) activity, FOA, and ictal (ICT) activity; and (iii) FOA lies in the gamma frequency band as shown in the spectrograms.

Markers for the onset and offset of each period were added manually (see Figure 1C, red dashed lines): the PreICT period was defined as the 20 s preceding the FOA, and the ICT period extended from the end of the FOA to the end of the seizure. Finally, the analyzed data consisted of 30 pairs of bipolar SEEG signals (10 patients, three pairs per patient), each segmented into interictal, PreICT, FOA, and ICT periods.

2.2 | SEEG signal processing

2.2.1 | Time–frequency analysis

Signal processing was performed using the Amadeus software.[17] The signals were pre-processed with a 1–200 Hz

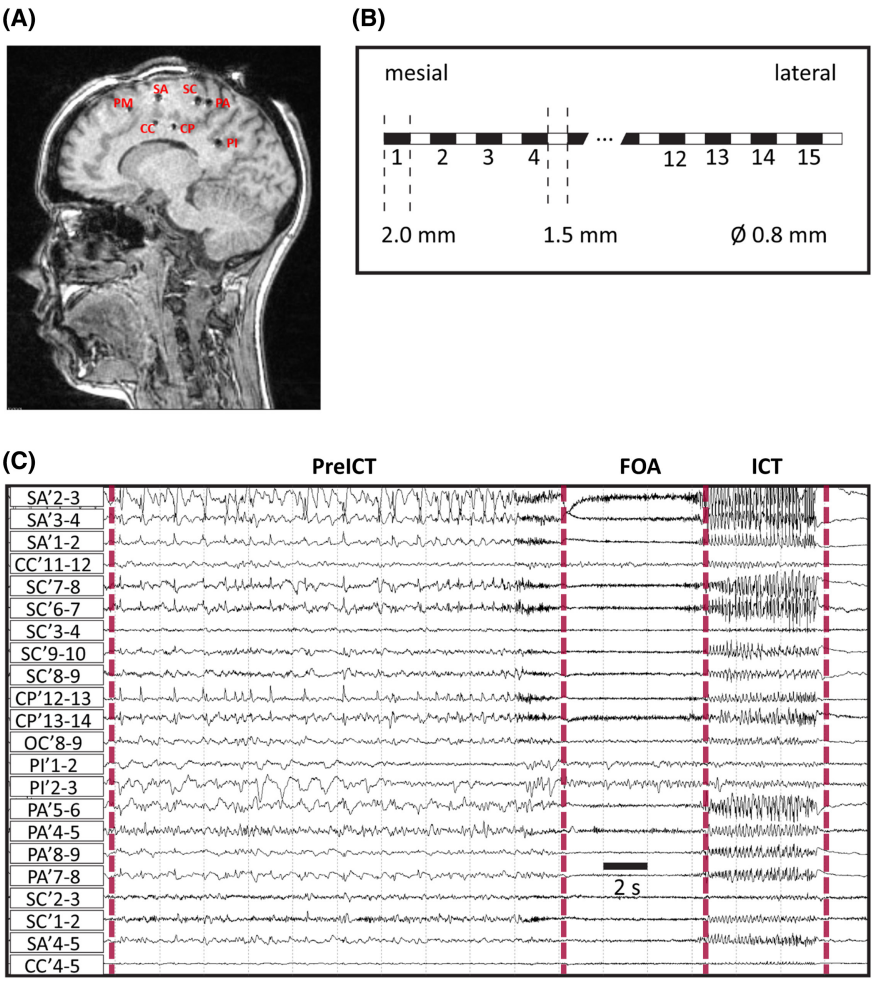

FIGURE 1 SEEG presurgical investigation in drug-resistant focal epilepsy. (A) Sagittal MRI view showing the position and names of the eight implanted electrodes. (B) Schematic diagram of the intracerebral electrode. Electrode contacts are 2 mm long, .8 mm in diameter, and 1.5 mm apart. They are numbered. Low numbers refer to contacts located in mesial brain structures. High numbers refer to contacts located in lateral structures. (C) SEEG signals recorded during the interictal–ictal transition. Capital letters refer to the name of brain structures. For simplicity, only channels disclosing epileptic activity are shown. In epileptogenic regions, signals are characterized by three distinct phases: pre-ictal (PreICT), fast-onset activity (FOA), and ictal (ICT), which are delineated by red dashed lines.

bandpass filter to remove the non-physiological very slow waves and fast ripples (>200 Hz), which are not the focus of this study. For the three different periods (PreICT, FOA, and ICT), the relative power spectral density was calculated for each frequency sub-band classically defined for EEG, namely theta [4–8 Hz[, alpha [8–13 Hz[, beta [13–24 Hz], and gamma/high gamma (>24 Hz).[18]

The energy ratio in the beta-gamma frequency sub-band relative to the theta-alpha sub-band was used to determine the onset and the offset of the FOA period, as described in the epileptogenicity index method.[8]

2.2.2 | Non-linear correlation analysis

We estimated functional connectivity using the non-linear correlation coefficient $h^2_{X;Y}$, which quantifies the interdependence between signals X and Y.[19,20] This method was introduced originally for the analysis of brain signals by Lopes da Silva and colleagues,[21] and further applied to multidimensional signals by Kalitzin and colleagues.[22]

$$h^2_{X;Y}(\tau) = \max_{\tau_{\min} < \tau < \tau_{\max}} \left\{ 1 - \frac{\mathrm{VAR}[Y(t+\tau)|\, X(t+\tau)]}{\mathrm{VAR}[Y(t+\tau)]} \right\} \quad (1)$$

where τ is the time shift. As initially proposed,[21] the $h^2_{X;Y}$ coefficient was calculated at the maximal time shift. Here, time delay values and directionality indices were not analyzed, as the objective was to primarily emphasize the "synchronization, de-synchronization, and re-synchronization" pattern. The $h^2_{X;Y}$ coefficient takes values between 0 (signals X and Y are independent) and 1 (signal Y is completely determined by signal X). $h^2_{X;Y}$ Values were calculated over a window of 1 s, sliding by steps of 0.25 s.

For all patients, the $h^2_{X;Y}$ values were calculated for all pairwise combinations of signals from three distant neocortical structures: $h^2_{\mathrm{sig}_1;\mathrm{sig}_2}, h^2_{\mathrm{sig}_1;\mathrm{sig}_3}, h^2_{\mathrm{sig}_2;\mathrm{sig}_3}$. Figure 2 illustrates the patient's SEEG signals (Patient 2), complemented by corresponding spectrograms showing the color-coded signal energy for successive periods of interest (PreICT, FOA, and ICT). Figure 2C shows the time evolution of the non-linear correlation, revealing a typical (de)synchronization pattern during the PreICT to ICT period, passing through the FOA period.

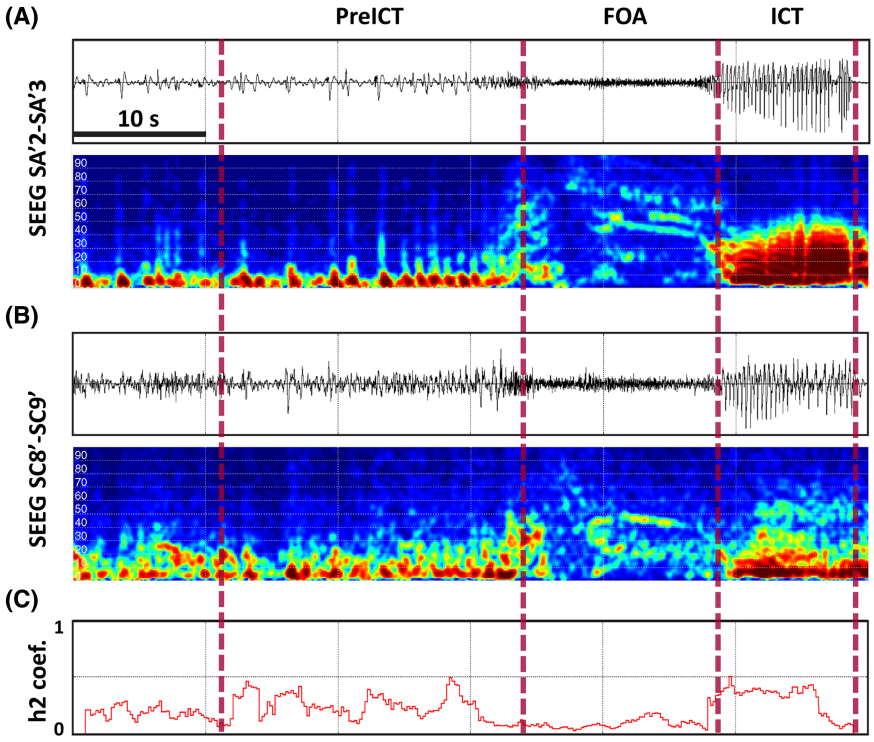

FIGURE 2 A zoom in SEEG signals recorded during the interictal–ictal transition. (A, top panel) Bipolar signal recorded from the mesial contacts (2, 3) of the electrode implanted in the Supplementary Area (SA). (A, bottom) Time-frequency representation (spectrogram) of the SEEG signal. Hot colors denote high energy levels. The fast-onset activity (FOA) period is characterized by the appearance of a rapid discharge in the gamma frequency bands (~30–70 Hz, as observed in both spectrograms). (B, top panel) Bipolar signal recorded from the lateral contacts (8, 9) of the electrode implanted in the Central Sulcus (SC). (B, bottom) Time-frequency representation (spectrogram) of the SEEG signal. The rapid discharge occurs quasi simultaneously on electrode contacts SA′2–3 and SC′8–9. (C) Non-linear correlation (h^2) values (computed on a 1 s window sliding by steps of .25 s) showing the decorrelation of SEEG activity occurring during the FOA period, just after PreICT phase and before the ICT phase.

2.3 | Statistical analysis

For each patient, we selected three bipolar signals divided into PreICT, FOA, and ICT periods. For a given period, we pooled the h^2 values calculated over the sliding window for each of the three pairs obtained with the three selected signals:

$$h^2_{\text{pooled}}(\text{period}) = h^2_{\text{sig}_1;\text{sig}_2}(\text{period}), h^2_{\text{sig}_1;\text{sig}_3}(\text{period}), h^2_{\text{sig}_2;\text{sig}_3}(\text{period}), \quad (2)$$

where period = {PreICT; FOA; ICT}

To compare non-linear correlation values, first, a one-way analysis of variance (ANOVA) test (Kruskal–Wallis) was performed to assess possible statistical differences in h^2 values between the three periods of interest. The Kruskal–Wallis test was used because the compared values do not meet the assumption of normal distribution. Then, a post hoc Dunn's test was performed to determine which specific time periods differed significantly from each other. A significance threshold of 1% was chosen and the family-wise error rate was controlled using the Bonferroni method. Statistical tests were performed using the Python Scipy package.

2.4 | Computational modeling of SEEG signals

2.4.1 | Model description

We considered a network of two distant neuronal populations, each representing a neocortical region. The reader is referred to Table SI2 for a detailed description of the model equations. Figure 3A shows the single population model. This model can accurately simulate real patient signals by adjusting parameter values, as demonstrated in Figure 3B, which compares the simulated SEEG signal with that of a patient, showing very similar activity during the PreICT, FOA, and ICT periods. Figure 4A illustrates two neuronal populations labeled P1 and P2. These populations are symmetrically connected.

Dynamical changes of model parameters were optimized by visual comparison of simulated and real signals,

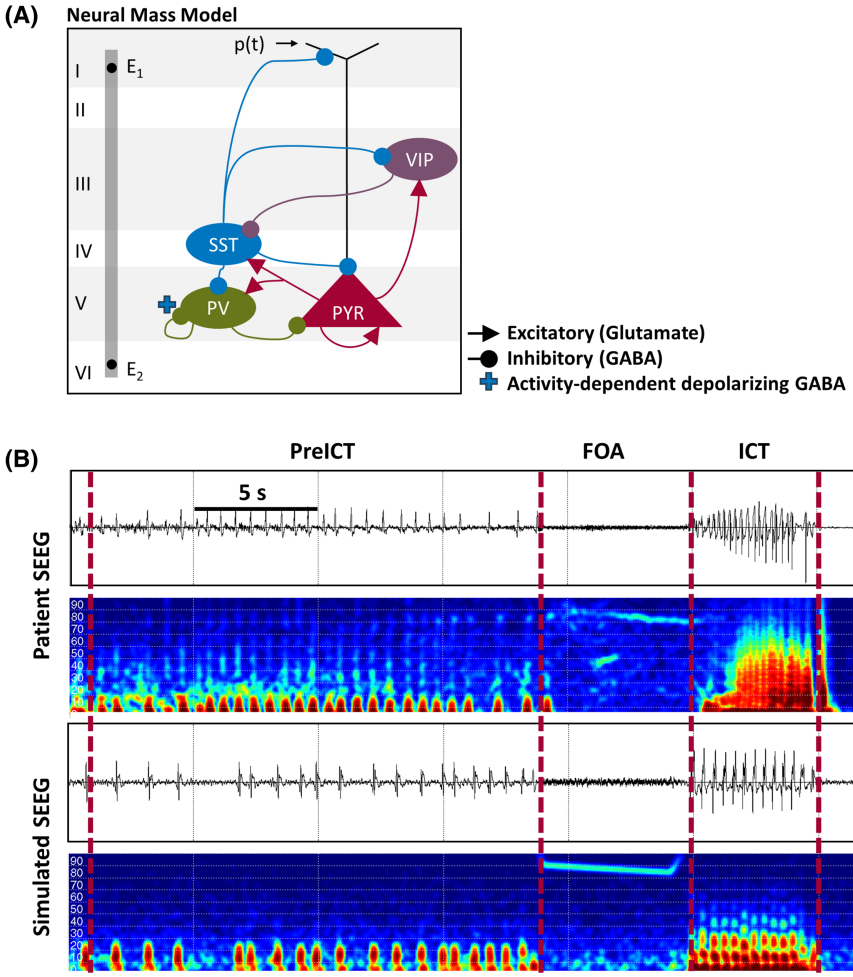

FIGURE 3 Neuro-inspired layered neuronal population model simulating the local activity of one region of the neocortex. (A) The model includes one subpopulation of glutamatergic pyramidal cells (PYR, red triangle) and three subpopulations of GABAergic interneurons (VIP, SST, and PV ellipses). Neuronal sub-populations are located in specific layers (I–VI) of the neocortex. The connectivity among subpopulations is derived from the literature. The Gaussian white noise p(t) accounts for non-specific excitatory afferences to the neuronal population. To approximate the local field potential recorded at the SEEG electrode contacts, two monopoles in opposite directions were considered to account for current sinks and sources occurring in response to synaptic activation of PYR cells, either at basal or apical dendrites. (B) Real and simulated SEEG signals along with corresponding spectrograms.

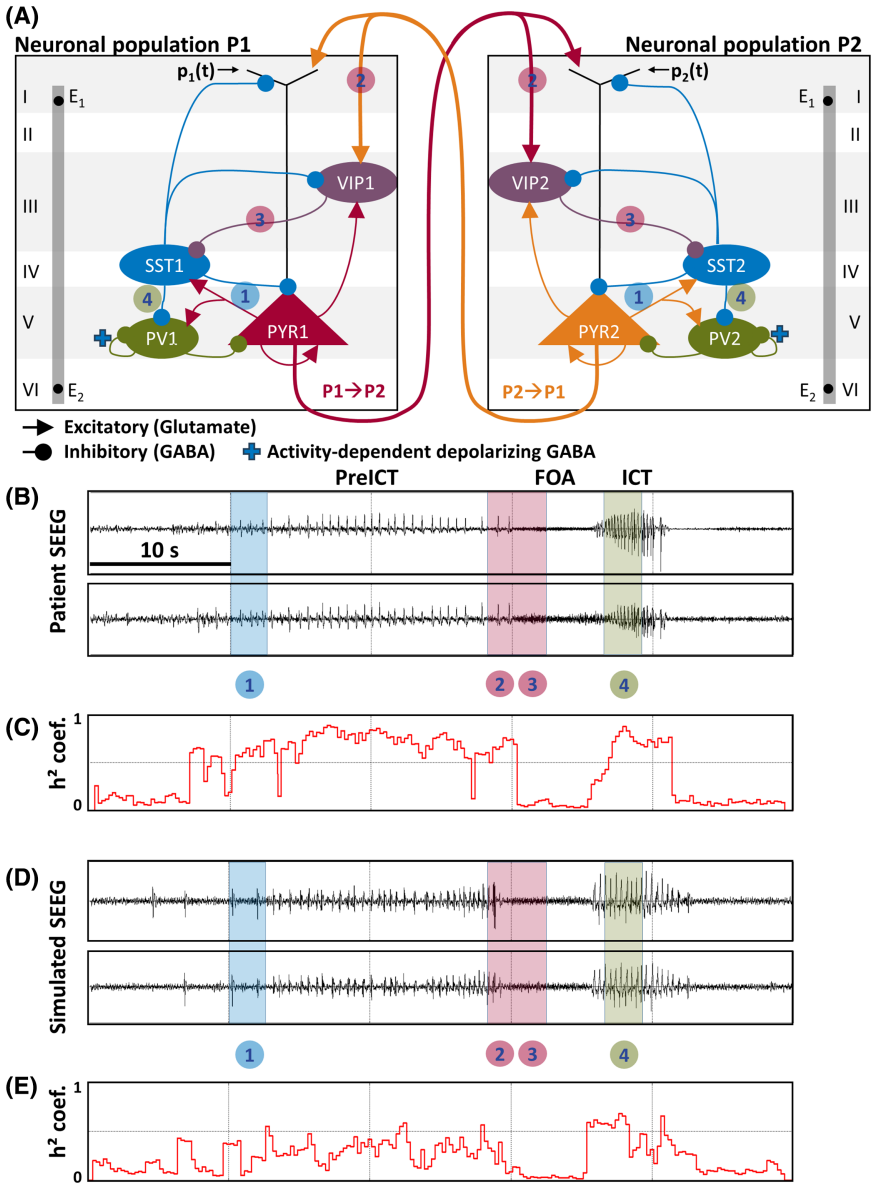

FIGURE 4 SEEG simulation from the model of two coupled distant neuronal populations (P1 and P2). (A) The neuronal populations are bidirectionally interconnected. Connections include (i) long-range excitatory projections from the PYR cells subpopulation of P1 (resp. P2) onto the PYR cells subpopulation of P2 (resp. P1) and (ii) long-range excitatory projections from the PYR cells subpopulation of P1 (resp. P2) onto the VIP interneurons subpopulation of P2 (resp. P1). The numbers 1–4 in colored disks indicate the successive key steps, which explain the transition from interictal to ictal activity (see text for details, Section 3). (B) Patient SEEG signals recorded from two brain structures and (C) corresponding non-linear correlation (h^2) values. (D) SEEG signals simulated from the model and (E) corresponding non-linear correlation (h^2) values. Highlighted areas denote the transitions between different activities (blue: interictal to PreICT; pink: PreICT to FOA; green: FOA to ICT).

complemented by signal processing (spectrograms). The successive phases of interictal–ictal transition were obtained under the following constraints: (i) transitions are obtained by varying a minimum number of parameters; (ii) the frequency and duration of the simulated activities are similar to key features of the patient signals, such as interictal spiking at 3 Hz, low-voltage fast activity at about 70 Hz with chirping phenomenon, and ictal activity at 3 Hz with higher amplitude than the interictal spikes; (iii) decorrelation of signals is observed during fast onset activity (quantified by $h^2_{X;Y}$ values); and, finally, (iv) pyramidal cell average activity is reduced during the fast onset activity, whereas GABAergic fast-spiking interneuron activity is increased.

It is noteworthy that a limited set of six parameters (Table SI2.1) proved to be necessary and sufficient to reproduce the observed SEEG signals recorded during the transition to seizure. Along the same lines, other model parameters such as the rise and decay times of excitatory/inhibitory postsynaptic potentials were set to known constant values.

Finally, the simulated data consisted of 10 pairs of simulated SEEG signals obtained by varying the mean and variance of the model input noise ($p_1(t)$, $p_2(t)$) by 10%. The stochastic ordinary differential equations governing the dynamics of the model were solved using the Euler–Maruyama method with a time step of 1/2048 s. The h^2 non-linear correlation coefficient was calculated for each pair of simulated signals and the statistical analysis was performed on the ensemble of simulations (see Section 2.3).

3 | RESULTS

3.1 | Patient data analysis

The SEEG signals collected from patients ($n = 10$) showed rather stereotyped interictal and ictal patterns with different durations. A representative example is shown in Figure 4B. SEEG signals included pre-ictal spikes and sustained ictal spiking, although some patients had noticeably shorter or longer epochs of spiking activity in either the PreICT, the ICT, or both periods. An increase of spiking frequency marked the PreICT period (which lasted 20 s, by definition). It was followed by the FOA period, which lasted 4.5 s on average (standard deviation [SD] = 1.2 s). The subsequent ICT period lasted 40 s on average (SD = 37.1 s). Seizure termination was always abrupt. The SD for the ICT period indicated a large variance in duration. The spiking frequency in the PreICT and ICT periods could be as low as 2 Hz and as high as 15 Hz. In general, the ICT period had a significantly higher spiking amplitude and frequency than the PreICT period.

Seizure onset was characterized predominantly by a fast activity in the gamma range (24–80 Hz), with a chirp observed in the majority of cases (8 of 10 patients), characterized by a progressive decrease in frequency by ~5–10 Hz. The low-voltage nature of the signals at seizure onset was present in all patients except for Patient 1, in whom a higher amplitude FOA was observed.

3.2 | Simulated data analysis

The simulated SEEG signals showed characteristics similar to those observed in the patient signals. In the pre-ictal period, our model showed an average spiking frequency of 2 Hz. In contrast, in the ictal period, an average spiking frequency of 6 Hz was observed, with a noticeably higher spiking amplitude, as in real signals. Figure 4D shows an example of two simulated SEEG signals for model parameters identified from the two real signals displayed in Figure 4B. For appropriate tuning of the model parameters, the sequences of simulated SEEG patterns occurring during the PreICT, FOA, and ICT periods were found to be similar to those observed in the patient signals. The simulated signals showed a fast activity (gamma range) at seizure onset, which started simultaneously in both neuronal populations at $t = 30$ s, and lasted for 5 s. Seizure onset was characterized by a significant decrease in h^2 values, which increased again at the beginning of the ictal state (Figure 4E), as similarly observed in the patients' SEEG signals (Figure 4C).

Bidirectional connections between the two neuronal populations were found to be the key actors in the transition to seizure and the emergence of fast activity at seizure onset. In the model, the conditions necessary to reproduce the four steps of the interictal–ictal transition are illustrated in Figure 4A and summarized below:

Step 1: The transition was triggered by the disinhibition of pyramidal (PYR) cells, simulated by a 15% reduction in both neuronal populations of the amplitude of inhibitory postsynaptic potentials (IPSPs) mediated by GABAergic somatostatine positive (SST) interneurons onto PYR cells (parameter $\boldsymbol{W}_{\boldsymbol{SST_B}}$). This reduction resulted in an increase of excitability and amplified the occurrence of epileptic spikes, causing the system to enter the PreICT phase. **Step 2:** The subsequent increase of glutamatergic input from PYR cells to distant vaso-intestinal peptide positive (VIP) interneurons ($\boldsymbol{C}_{\boldsymbol{PYR_1 \rightarrow VIP_2}}$ and $\boldsymbol{C}_{\boldsymbol{PYR_2 \rightarrow VIP_1}}$) amplified the activity of inhibitory VIP interneurons in both neuronal populations. **Step 3:** In turn, this increased activity of VIP interneurons inhibited the activity of SST interneurons (SST_1 and SST_2). This inhibition of SST_1 and SST_2 interneurons led to (i) the disinhibition of parvalbumin positive (PV) interneurons (PV_1 and PV_2) and (ii) the simultaneous activation of pyramidal-interneuron-gamma (PING) networks in both neuronal populations (PYR_1-PV_1 and PYR_2-PV_2). The massive increase of the firing rate of PV interneurons explained (i) the appearance of the FOA and (ii) the SEEG decorrelation pattern explained by the silencing of PYR cells by PV interneurons (Figure 5B,

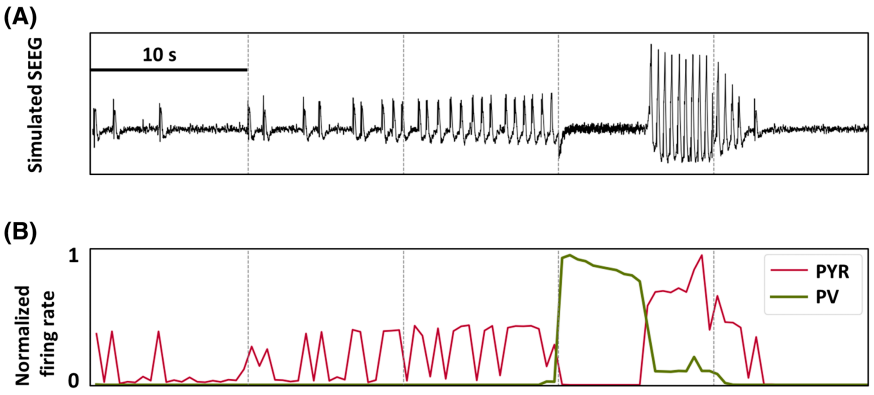

FIGURE 5 Behavior of pyramidal cells and PV interneurons during the interictal to ictal transition. (A) Simulated SEEG signal. (B) corresponding firing rate of PYR cells (red line) and PV interneurons (green line). Firing rates were averaged over a sliding window of 100 ms. The firing rates of other interneurons are omitted due to their negligible activity during the FOA.

red curve). Simultaneously with the activation of PV interneurons, two other factors were activated: the depolarizing GABA phenomenon by using a negative value of parameters $C_{PV' \to PV}$ and $C_{PV \to PV'}$ (Table SI2.1) in both distant neuronal populations further reducing the seizure threshold of the system, and the autaptic connectivity of PV interneurons ($C_{PV \to PV}$) was increased to modulate the frequency of the FOA phase. **Step 4:** Finally, the firing rate of PV interneurons (PV_1 and PV_2) gradually decreased during the FOA (Figure 5B, green curve). This reduction led to the reactivation of PYR cells (PYR1 and PYR2) in both populations, producing a spiking activity characteristic of the ICT phase, marked by a resynchronization pattern in the SEEG signals, as quantified by non-linear correlation values (h^2 coefficient).

Of interest, a very small difference (2 ms) in the kinetics of fast IPSPs mediated by PV interneurons onto PYR cells was found to accentuate the decorrelation between signals simulated by the two coupled neuronal populations.

It is worth noting that the statistical analysis of the power spectral density and the non-linear correlation showed high agreement between simulated and real SEEG signals, as described below.

3.3 | Statistical analysis of patient and simulated signals

The relative average power per frequency sub-band was calculated for each patient. In Figure 6A, the summated signal power for all 10 patients for each sub-band was summarized as stacked histograms showing that during the FOA period, the average power was indeed distributed predominantly in the gamma band (24–80 Hz), in contrast to the PreICT and ICT periods where the power was distributed predominantly in the theta and alpha bands (4–8 Hz and 8–13 Hz). The summated power between all three pairs of SEEG signals per patient was also calculated (Figure SI3.1), which showed similar trends for individual patients as in summated signal power for all patients.

Figure 6A shows the boxplots of non-linear correlation values merged for the 10 patients and each period of interest (PreICT, FOA, ICT). A significant difference was observed between the PreICT and FOA periods and between the FOA and ICT periods.

Individual statistical tests (Figure SI3.1) indicate significant differences between the PreICT and the FOA periods and between the FOA and ICT periods in 9 of 10 patients. In addition, no significant difference was observed between the h^2 values of the PreICT and ICT periods in 5 of 10 patients.

In Figure 6B, the results of the same statistical tests applied to simulated SEEG signals (combined h^2 values for the 10 simulations) were found to mirror the observations made in the patient data, also highlighting a significant difference between the PreICT and FOA periods and between the FOA and ICT periods.

4 | DISCUSSION

4.1 | Dynamic changes in the connectivity pattern

The transition from interictal to ictal states in human focal seizures has long been a central topic in epileptology.[2,23] In patient signals, sporadic interictal spikes become more and more frequent and synchronous before the seizure starts with FOA preceded by large-amplitude synchronous spikes. These observations, also reported in literature,[24] suggest that this progressive synchronization between distant epileptogenic regions is not driven

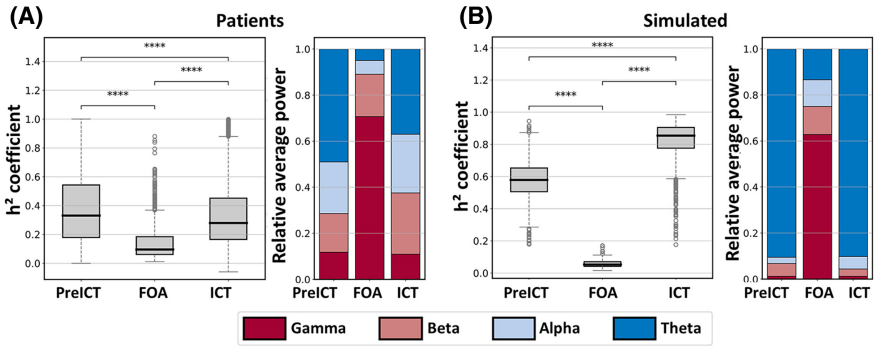

FIGURE 6 Comparison of average non-linear correlation values and average power in frequency sub-bands for real and simulated signals. (A, left plot) Distribution of h^2 values computed from patient SEEG signals during the PreICT, FOA, and ICT periods and its post hoc Dunn's test were applied. $p > .01$: ns (not significant); $10^{-2} > p > 10^{-3}$: *; $10^{-3} > p > 10^{-4}$: **; $10^{-4} > p > 10^{-5}$: ***; $p < 10^{-5}$: ****. (A, right plot) The average SEEG signal power in each sub-band (theta, alpha, beta, and gamma) computed for the group of patients. (B, left plot) Distribution of h^2 values computed from simulated SEEG signals during the PreICT, FOA, and ICT periods.

by an external trigger but rather is caused by the gradual increase of excitation in remote regions resulting from reciprocal glutamatergic inputs.

We consistently measured a decrease in correlation during the FOA period as reported in previous studies,[14] followed by a marked increase during the ICT period characterized by the appearance of high-amplitude spiking activity in the theta and alpha bands These results are in line with the "synchronization, de-synchronization, re-synchronization" pattern described in previous clinical studies and hypothesized to be a hallmark of the seizure-onset zone.[6,13,14] They suggest that the rapid discharge corresponds to a transient (4–8 s) phase of decoupling between brain structures that occurs between two states of hypersynchronous activity.

4.2 | The key role of GABAergic networks in the interictal–ictal transition

In the model, the circuitry of neocortical regions remains the same in the non-epileptic brain. The main differences occur at the level of synaptic transmission, keeping in mind that epileptogenicity is caused by a number of factors, often complex and acting synergistically, as reported in many studies.[25,26] The transition from the interictal to ictal state is first facilitated by a gradual decrease of dendritic inhibition mediated by SST interneurons on PYR cells at the level of slow GABA receptors. Regarding the specific transition from the PreICT to the FOA period, the model sheds light on the crucial role of GABAergic interneurons (especially fast-spiking PV interneurons), in line with a number of in vitro[27] and in vivo studies.[7,9,28]

Following on this theme, the model also confirmed the key role of parameters in shaping of the FOA, namely the depolarizing GABA mechanism, which was implemented in the model by switching the sign of parameters $C_{PV' \to PV}$ and $C_{PV \to PV'}$ and the mutual inhibition between PV interneurons $C_{PV \to PV}$. The former favors the occurrence of the FOA events, whereas the latter controls the FOA frequency (24–80 Hz). These mechanistic findings are consistent with the results described in Deleuze et al.,[29] suggesting that the strong autaptic self-connectivity of neocortical PV interneurons facilitates their tuning to oscillations in the gamma frequency band (24–80 Hz).

In the model, the impact of the depolarizing GABA mechanism is simulated by positive IPSPs[30] and implemented by switching the sign of parameters $C_{PV' \to PV}$ and $C_{PV \to PV'}$. It can be attributed to the downregulation of the K^+/Cl^- ion co-transporter KCC2,[31] resulting in a net accumulation of intracellular chloride concentrations, and in a shift in the reversal potential for chloride.[32]

Moreover, the model is able to capture an important aspect of the FOA: The activity of PYR cells is silenced, whereas GABAergic PV interneurons have an increased firing rate. This phenomenon was observed in different experimental studies.[7,9,27,33] The model predicts (i) that this increased activity of PV interneurons is due to the concurrent depolarizing GABA mechanism and disinhibition by VIP interneurons, and (ii) that consequently the silencing of PYR cells activity is due to the massive GABAergic inhibition caused by the increased PV interneuron activity.

4.3 | The key role of VIP interneurons in the simultaneous occurrence of FOA in distant brain regions

The proposed model for the interictal-to-ictal transition is based on the premise of a local disinhibition pathway between VIP, SST, and PV. This local pathway is consistent with known inhibitory connections in the neocortex.[34] Furthermore, long-range glutamatergic input to GABAergic VIP interneurons has also been reported in a number of studies.[35,36] The disinhibitory effect of VIP interneurons has been investigated in vitro.[37–39]

In the model, the increased excitatory input from PYR cells to distant VIP interneurons provides an explanation for an intriguing feature: the quasi-simultaneous occurrence of the FOA in distant regions, whereas there is a decorrelation between locally-recorded SEEG activity.[6] The proposed model explains the mechanisms underlying this feature in terms of changes (i) between brain regions (increased glutamatergic input to VIP interneurons leading to increased GABA input on SST interneurons and thus, reduced SST interneuron activity) and (ii) within brain regions (increased activity of PV interneurons allowed by the reduction of SST activity, leading to fast activity in SEEG signals). Our modeling results suggest that this simultaneous occurrence of the FOA is not the result of a propagation mechanism, but is caused by similar pathological alterations of brain tissue. Thus the FOA is likely triggered by synchronized pre-ictal spikes that activate the same cascade of mechanisms in synaptically connected nodes of the EZN.

Furthermore, the role of VIP interneurons becomes critical in the context of seizure initiation, as indicated by Khoskhoo et al.,[40] who suggests that optogenetical inhibition of VIP interneurons increases seizure threshold, or shortens seizure duration. Similarly, a recent study by Rahimi et al.[41] elucidated the disinhibitory role of VIP interneurons in temporal lobe epilepsy. The authors observed that silencing VIP interneurons dampened seizure activity, whereas short-term activation of VIP interneurons increased seizure activity. These in vivo studies corroborate

our modeling results regarding the increased signaling of VIP interneurons at seizure onset.

4.4 | Comparison with other computational modeling studies

Compared to previous studies that have used the same NMM formalism, we have included the VIP inhibitory interneurons, in addition to the fast (PV) and slow (SST) GABAergic interneurons.

In one study,[42] the authors identified key conditions for the model to reproduce the FOA observed in patients. They emphasized the critical role of connections between PYR cells and inhibitory fast spiking interneurons to simulate the high-frequency signal observed during FOA.

Fan et al.[43] optimized three main parameters of a single population NMM for SEEG data in 10 patients with temporal lobe epilepsy. They found that the excitation/fast inhibition ratio increased around seizure onset in contrast to the excitation/slow inhibition ratio, which decreased before seizure termination. In our model, we converged to the same parameter evolution by gradually decreasing the IPSPs mediated by SST interneurons.

5 | LIMITATIONS

To implement the depolarizing GABA mechanism, we added GABA receptors with positive IPSPs (instead of negative). In addition, we implemented depolarizing GABA effects only at the level of PV interneurons and not at the level of PYR cells, as reported in Herrmann et al.[44] A more-refined approach to implementing depolarizing GABA involves making relevant parameters of the model time-dependent, to obtain a dynamic effect.[30,45]

Our model can also be extended to explicitly represent the dynamics of extracellular and intracellular ion levels, which are known to promote epileptic oscillations during the interictal–ictal transition.[46] Avoli et al.[47] proposed that the excessive activation of GABA receptors leads to an abnormal increase in extracellular potassium concentration, triggering FOA at seizure onset.

6 | CONCLUSION

We analyzed the mechanisms underlying the interictal–ictal transition in patients with focal epilepsy, from SEEG signals. We proposed a novel model that can replicate the observed sequence of SEEG patterns with high fidelity. This model highlights the variations of key parameters for which the chirp-like oscillations in the gamma frequency range can match patient SEEG recordings at the onset of focal seizures. This model has the advantage of being grounded in neurobiology and neurophysiology, which enhances its explanatory value: the number of scenarios leading to the desired simulated signal features was found to be limited, emphasizing the uniqueness and relevance of the mechanistic insights gained.

AUTHOR CONTRIBUTIONS

Conceptualization: Fabrice Wendling, Fabrice Bartolomei. *Data curation*: Mehmet Alihan Kayabas, Fabrice Wendling. *Methodology*: Mehmet Alihan Kayabas, Fabrice Wendling, Pascal Benquet. *Formal analysis, research, validation, visualization*: Mehmet Alihan Kayabas, Elif Köksal Ersöz, Pascal Benquet, Fabrice Wendling. *Software development*: Maxime Yochum, Elif Köksal Ersöz. *Writing and editing*: Mehmet Alihan Kayabas, Fabrice Wendling, Elif Köksal Ersöz. *Reviewing*: All co-authors. All authors have approved the submitted version of this article.

ACKNOWLEDGMENTS

This project has received funding from the European Research Council (ERC) under the European Union's Horizon 2020 research and innovation program (Grant agreement no. 855109).

CONFLICT OF INTEREST STATEMENT

The authors declare no conflicts of interest.

DATA AVAILABILITY STATEMENT

The data supporting this study will be openly available in a secured repository upon reasonable request to the corresponding author, after publication of the results. The data will include the set of simulated SEEG signals generated for typical scenarios of the interictal-to-ictal transition. The Python source code for simulating SEEG signals reproducing real signals during interictal, preictal, seizure onset, and ictal activity will also be provided.

ETHICS STATEMENT

We confirm that we have read the Journal's position on issues involved in ethical publication and affirm that this report is consistent with those guidelines.

ORCID

Elif Köksal Ersöz https://orcid.org/0000-0003-3696-7953
Maxime Yochum https://orcid.org/0000-0001-8632-6041
Fabrice Bartolomei https://orcid.org/0000-0002-1678-0297

REFERENCES

1. Bartolomei F, Lagarde S, Wendling F, McGonigal A, Jirsa V, Guye M, et al. Defining epileptogenic networks: contribution of SEEG and signal analysis. Epilepsia. 2017;58(7):1131–47.
2. Lagarde S, Buzori S, Trebuchon A, Carron R, Scavarda D, Milh M, et al. The repertoire of seizure onset patterns in human focal epilepsies: determinants and prognostic values. Epilepsia. 2019;60(1):85–95.
3. Grinenko O, Li J, Mosher JC, Wang IZ, Bulacio JC, Gonzalez-Martinez J, et al. A fingerprint of the epileptogenic zone in human epilepsies. Brain. 2018;141(1):117–31.
4. Bancaud J, Angelergues R, Bernouilli C, et al. Functional stereotaxic exploration (SEEG) of epilepsy. Electroencephalogr Clin Neurophysiol. 1970;28(1):85–6.
5. Fisher RS, Webber WR, Lesser RP, Arroyo S, Uematsu S. High-frequency EEG activity at the start of seizures. J Clin Neurophysiol. 1992;9(3):441–8.
6. Wendling F, Bartolomei F, Bellanger JJ, Bourien J, Chauvel P. Epileptic fast intracerebral EEG activity: evidence for spatial decorrelation at seizure onset. Brain. 2003;126(Pt 6):1449–59.
7. Elahian B, Lado NE, Mankin E, Vangala S, Misra A, Moxon K, et al. Low-voltage fast seizures in humans begin with increased interneuron firing. Ann Neurol. 2018;84(4):588–600.
8. Bartolomei F, Chauvel P, Wendling F. Epileptogenicity of brain structures in human temporal lobe epilepsy: a quantified study from intracerebral EEG. Brain. 2008;131(Pt 7):1818–30.
9. de Curtis M, Avoli M. GABAergic networks jump-start focal seizures. Epilepsia. 2016;57(5):679–87.
10. Shiri Z, Levesque M, Etter G, Manseau F, Williams S, Avoli M. Optogenetic low-frequency stimulation of specific neuronal populations abates ictogenesis. J Neurosci. 2017;37(11):2999–3008.
11. Yekhlef L, Breschi GL, Lagostena L, Russo G, Taverna S. Selective activation of parvalbumin- or somatostatin-expressing interneurons triggers epileptic seizurelike activity in mouse medial entorhinal cortex. J Neurophysiol. 2015;113(5):1616–30.
12. Zhang ZJ, Valiante TA, Carlen PL. Transition to seizure: from "macro"- to "micro"-mysteries. Epilepsy Res. 2011;97(3):290–9.
13. Mormann F, Kreuz T, Andrzejak RG, David P, Lehnertz K, Elger CE. Epileptic seizures are preceded by a decrease in synchronization. Epilepsy Res. 2003;53(3):173–85.
14. Bartolomei F, Wendling F, Regis J, Gavaret M, Guye M, Chauvel P. Pre-ictal synchronicity in limbic networks of mesial temporal lobe epilepsy. Epilepsy Res. 2004;61(1–3):89–104.
15. Talairach J, Bancaud J, Szikla G, Bonis A, Geier S, Vedrenne C. New approach to the neurosurgery of epilepsy. Stereotaxic methodology and therapeutic results. 1. Introduction and history. Neurochirurgie. 1974;20(Suppl 1):1–240.
16. Wendling F, Badier JM, Chauvel P, Coatrieux JL. A method to quantify invariant information in depth-recorded epileptic seizures. Electroencephalogr Clin Neurophysiol. 1997;102(6):472–85.
17. Wendling F, Badier JM. Clinical engineering in neurophysiology: an object-oriented platform for signal visualization and processing. J Clin Eng. 1998;23(3):189–95.
18. Schomer DL, Da Silva FHL. Niedermeyer's electroencephalography: basic principles, clinical applications, and related fields. 6th ed. Lippincott Williams & Wilkins (LWW): Li-ppincott Williams & Wilkins; 2011.
19. Wendling F, Bartolomei F, Bellanger JJ, Chauvel P. Interpretation of interdependencies in epileptic signals using a macroscopic physiological model of the EEG. Clin Neurophysiol. 2001;112(7):1201–18.
20. Wendling F, Chauvel P, Biraben A, Bartolomei F. From intracerebral EEG signals to brain connectivity: identification of epileptogenic networks in partial epilepsy. Front Syst Neurosci. 2010;4:154.
21. Lopes da Silva F, Pijn JP, Boeijinga P. Interdependence of EEG signals: linear vs. nonlinear associations and the significance of time delays and phase shifts. Brain Topogr. 1989;2(1–2):9–18.
22. Kalitzin SN, Parra J, Velis DN, Lopes da Silva FH. Quantification of unidirectional nonlinear associations between multidimensional signals. IEEE Trans Biomed Eng. 2007;54(3):454–61.
23. Lagarde S, Bartolomei F. Focal epilepsies and focal disorders. Handb Clin Neurol. 2019;161:17–43.
24. Levesque M, Ragsdale D, Avoli M. Evolving mechanistic concepts of epileptiform synchronization and their relevance in curing focal epileptic disorders. Curr Neuropharmacol. 2019;17(9):830–42.
25. Magloire V, Mercier MS, Kullmann DM, Pavlov I. GABAergic interneurons in seizures: investigating causality with optogenetics. Neuroscientist. 2019;25(4):344–58.
26. Engel J Jr. Excitation and inhibition in epilepsy. CJNS. 1996;23(3):167–74.
27. Gnatkovsky V, Librizzi L, Trombin F, de Curtis M. Fast activity at seizure onset is mediated by inhibitory circuits in the entorhinal cortex in vitro. Ann Neurol. 2008;64(6):674–86.
28. Neumann AR, Raedt R, Steenland HW, Sprengers M, Bzymek K, Navratilova Z, et al. Involvement of fast-spiking cells in ictal sequences during spontaneous seizures in rats with chronic temporal lobe epilepsy. Brain. 2017;140(9):2355–69.
29. Deleuze C, Bhumbra GS, Pazienti A, Lourenço J, Mailhes C, Aguirre A, et al. Strong preference for autaptic self-connectivity of neocortical PV interneurons facilitates their tuning to gamma-oscillations. PLoS Biol. 2019;17(9):e3000419.
30. Kurbatova P, Wendling F, Kaminska A, Rosati A, Nabbout R, Guerrini R, et al. Dynamic changes of depolarizing GABA in a computational model of epileptogenic brain: insight for Dravet syndrome. Exp Neurol. 2016;283:57–72.
31. Kaila K, Price TJ, Payne JA, Puskarjov M, Voipio J. Cation-chloride cotransporters in neuronal development, plasticity and disease. Nat Rev Neurosci. 2014;15(10):637–54.
32. Weiss SA. Chloride ion dysregulation in epileptogenic neuronal networks. Neurobiol Dis. 2023;177:106000.
33. Truccolo W, Donoghue JA, Hochberg LR, Eskandar EN, Madsen JR, Anderson WS, et al. Single-neuron dynamics in human focal epilepsy. Nat Neurosci. 2011;14(5):635–41.
34. Karnani MM, Jackson J. Interneuron cooperativity in cortical circuits. Neuroscientist. 2018;24(4):329–41.
35. Sun Q, Li X, Ren M, Zhao M, Zhong Q, Ren Y, et al. A whole-brain map of long-range inputs to GABAergic interneurons in the mouse medial prefrontal cortex. Nat Neurosci. 2019;22(8):1357–70.
36. Denoyer Y, Merlet I, Wendling F, Benquet P. Modelling acute and lasting effects of tDCS on epileptic activity. J Comput Neurosci. 2020;48(2):161–76.
37. Lee S, Kruglikov I, Huang ZJ, Fishell G, Rudy B. A disinhibitory circuit mediates motor integration in the somatosensory cortex. Nat Neurosci. 2013;16(11):1662–70.

38. Pfeffer CK, Xue M, He M, Huang ZJ, Scanziani M. Inhibition of inhibition in visual cortex: the logic of connections between molecularly distinct interneurons. Nat Neurosci. 2013;16(8):1068–76.
39. Pi H-J, Hangya B, Kvitsiani D, Sanders JI, Huang ZJ, Kepecs A. Cortical interneurons that specialize in disinhibitory control. Nature. 2013;503(7477):521–4.
40. Khoshkhoo S, Vogt D, Sohal VS. Dynamic, cell-type-specific roles for GABAergic interneurons in a mouse model of optogenetically inducible seizures. Neuron. 2017;93(2):291–8.
41. Rahimi S, Salami P, Matulewicz P, Schmuck A, Bukovac A, Ramos-Prats A, et al. The role of subicular VIP-expressing interneurons on seizure dynamics in the intrahippocampal kainic acid model of temporal lobe epilepsy. Exp Neurol. 2023;370:114580.
42. Molaee-Ardekani B, Benquet P, Bartolomei F, Wendling F. Computational modeling of high-frequency oscillations at the onset of neocortical partial seizures: from 'altered structure' to 'dysfunction'. NeuroImage. 2010;52(3):1109–22.
43. Fan X, Gaspard N, Legros B, Lucchetti F, Ercek R, Nonclercq A. Dynamics underlying interictal to ictal transition in temporal lobe epilepsy: insights from a neural mass model. Eur J Neurosci. 2018;47(3):258–68.
44. Herrmann T, Gerth M, Dittmann R, Pensold D, Ungelenk M, Liebmann L, et al. Disruption of KCC2 in Parvalbumin-positive interneurons is associated with a decreased seizure threshold and a progressive loss of Parvalbumin-positive interneurons. Front Mol Neurosci. 2021;14:807090.
45. Lopez-Sola E, Sanchez-Todo R, Lleal E, Köksal-Ersöz E, Yochum M, Makhalova J, et al. A personalizable autonomous neural mass model of epileptic seizures. J Neural Eng. 2022;19(5):ac8ba8.
46. Buchin A, Chizhov A, Huberfeld G, Miles R, Gutkin BS. Reduced efficacy of the KCC2 cotransporter promotes epileptic oscillations in a subiculum network model. J Neurosci. 2016;36(46):11619–33.
47. Avoli M, de Curtis M, Gnatkovsky V, Gotman J, Köhling R, Lévesque M, et al. Specific imbalance of excitatory/inhibitory signaling establishes seizure onset pattern in temporal lobe epilepsy. J Neurophysiol. 2016;115(6):3229–37.

SUPPORTING INFORMATION

Additional supporting information can be found online in the Supporting Information section at the end of this article.

How to cite this article: Kayabas MA, Köksal Ersöz E, Yochum M, Bartolomei F, Benquet P, Wendling F. Transition to seizure in focal epilepsy: From SEEG phenomenology to underlying mechanisms. Epilepsia. 2024;00:1–12. https://doi.org/10.1111/epi.18173